AIAA JOURNAL
Vol. 41, No. 12, December 2003

Thermomechanical Postbuckling Response and First-Ply Failure Analysis of Doubly Curved Panels

Maloy K. Singha,* L. S. Ramachandra,† and J. N. Bandyopadhyay‡
Indian Institute of Technology, Kharagpur 721 302, India

The thermomechanical postbuckling response of graphite/epoxy multilayered doubly curved (spherical and elliptic paraboloid) shell panels having rectangular planform is obtained within the framework of the finite element method. The nonlinear equilibrium paths are predicted using the displacement control method and the temperature-dependent material properties are used in the analysis. The structural model is based on a first-order shear deformation theory incorporating geometric nonlinearities. The first-ply failure of laminates is predicted with the Tsai–Wu failure criterion. Specific numerical results are reported that show the effects of radius-of-curvature-to-span ratio and thickness-to-span-ratio on the stability and strength characteristics of doubly curved shell panels subjected to combined thermal and mechanical loads. Moreover, numerical results are presented showing the effect of temperature dependence of material properties on limit loads and snap-through response of shallow curved panels.

Nomenclature

a, b	=	dimensions of the shell in plan
c	=	maximum rise of the spherical cap
E_L, E_T	=	Young's modulus in fiber and transverse-to-fiber directions
${}_te_{ij}, {}_t\eta_{ij}$	=	linear and nonlinear strains components
$\{F\}$	=	load vector
G_{LT}, G_{LZ}, G_{TZ}	=	shear modulus
${}^t\boldsymbol{g}_i$	=	covariant base vectors associated with convected coordinates r_i
h_k	=	shell thickness at node k
${}^n_nK_L$	=	linear strain incremental stiffness matrix
${}^n_nK_{\mathrm{NL}}$	=	nonlinear strain (geometric or initial stress) incremental stiffness matrix
N_k	=	interpolation functions associated with node k
P	=	nondimensional load parameter for uniformly distributed lateral pressure
P_c	=	central point load
Q	=	central concentrated load
q_0	=	intensity of the uniformly distributed lateral pressure
R, S, T	=	shear strengths of laminate
R_x, R_y	=	radius of curvatures along x and y directions, respectively
${}^{t+\Delta t}_{\ \ t}\ddot{S}^{ij}$	=	contravariant components of the second Piola–Kirchhoff stress tensor including thermal stresses
${}^tu_i$	=	displacement components at time t
${}^tV^k_{ni}$	=	normal to the shell midsurface at node k, of the N-noded ($N = 9,16$) isoparametric finite element
w_{central}	=	central displacement of the shell
X_T, X_C	=	tensile and compressive strength of the laminate in the fiber direction
${}^tx^k_i$	=	global coordinates of node k at time t
Y_T, Y_C	=	tensile and compressive strength of the laminate transverse to the fiber direction
α_k, β_k	=	rotation angles about two vectors ${}^t\boldsymbol{V}^k_1$ and ${}^t\boldsymbol{V}^k_2$, respectively
$\varepsilon^{\mathrm{AS}}_{ij}$	=	assumed strain fields
$\varepsilon^{\mathrm{DI}}_{ij}$	=	covariant components of Green–Lagrange strain tensor
ν	=	Poisson's ratio
${}^t\tau_{ij}$	=	Cauchy stress components
${}^{t+\Delta t}\Re$	=	virtual work of the applied loads

Introduction

THIN laminated composite panels are widely used in aerospace, defense, and other high-performance application areas because of their light weight, high stiffness, and strength and the ease with which they can be tailored to any shape. These composite shell panels are sometimes subjected to stresses due to temperature variations in addition to applied mechanical loads. In this paper an attempt is made to examine the stability and strength (first-ply failure load) characteristics of laminated composite panels on rectangular planform subjected to thermal and mechanical loads.

Thangaratnam et al.[1] analyzed the buckling of laminated composite cylindrical and conical shells under thermal loads by using the finite element method. Eslami et al.,[2] and Eslami and Javaheri[3] obtained the thermal buckling of thin cylindrical shells for a number of practical thermal loadings based on the Donnell and improved Donnell equations. Krizhevsky and Stavsky[4] investigated the buckling and postbuckling response of clamped shallow spherical shells with polar orthotropic layers subjected to uniform external pressure and a steady-state thermal field. A 10th-order system of nonlinear differential equations was obtained by considering five Mindlin-type displacements and they were solved using a modified relaxation procedure. Huang and Tauchert[5] carried out large displacement analysis of laminated flat, cylindrical, and doubly curved panels under thermal loads within the framework of the finite element method. Postcritical equilibrium paths were obtained via the arc-length method. Laminate strengths were also predicted with the Tsai–Hill criterion. Some laminates are found to undergo two snappings prior to failure. Later on, Huang and Tauchert[6] studied the response of doubly curved cross-ply laminated panels subjected to mechanical loading and temperature variations. The three-dimensional equilibrium equations, expressed in terms of displacements, were reduced to a system of coupled ordinary differential equations, which were then solved by using the power series method.

Birman and Bert[7] carried out buckling and postbuckling analyses of composite plates and cylindrical shells subjected to elevated

Received 12 April 2003; revision received 3 May 2003; accepted for publication 20 June 2003.

*Research Scholar, Department of Civil Engineering; currently Information Technology Analyst, Engineering Analysis Center of Excellence, John F. Welch Technology Center, Bangalore 560 066, India.
†Associate Professor, Department of Civil Engineering.
‡Professor, Department of Civil Engineering.

temperature and axial compression. Librescu and Souza[8] analyzed shear deformable simply supported flat panels subjected to temperature and edge loadings. In this paper, the authors studied the effect of number of layers, shear deformation, and geometric imperfections on the postbuckling path of the flat panels. In an accompanying paper, Librescu et al.[9] reported effects of tangential edge constraints on the thermomechanical postbuckling response of flat and shallow curved panels. The perturbation technique was used by Shen[10] to obtain the thermomechanical equilibrium paths of stiffened cylindrical shells. Noor and Peters[11] investigated the nonlinear response of symmetrically laminated cylindrical panels with cutouts subjected to a combination of thermal and pressure loading with edge shortening or edge shear. The authors employed the Sanders–Budiansky-type first-order shear deformation shell theory, which considers the effects of large displacement and moderate rotations in the analysis. A mixed formulation was employed with the fundamental unknowns consisting of the generalized displacements and shear resultants of the panel. In an interesting paper, Hause et al.[12] reported the thermomechanical buckling and postbuckling response of sandwich plates with anisotropic face sheets. The authors have shown by numerical examples that under certain complex loading conditions, the plate undergoes snap-through buckling. However, by judicious choice of directional properties of the face sheets they could eliminate the snap-through response of the plate altogether. Librescu et al.[13] presented an analytical study of the nonlinear response of simply supported flat and cylindrical panels subjected to preexisting, nondestabilizing lateral pressure, thermal loads, and mechanical edge loads. Results are presented for transversely isotropic, single-layer panels and three-layer sandwich panels that illustrate how the temperature field, initial imperfections, lateral pressure loads, and mechanical edge loads interact to change the character of the nonlinear shell response. Noor and Burton[14] and Argyris and Tenek[15] reviewed critically different computational models that were used in multilayered plate and shell analyses. In a review paper,[16] Thornton discusses the progress made in the field of thermal buckling of plates and shells. Apart from discussing the role of material thermal properties, the research in the area of thermal buckling of plates and shells is described in that paper, which lists around 126 references.

It is clear from the preceding discussion that due attention has not been given to the fact that mechanical properties degrade with rise in temperature. Also no results are available in the literature on postbuckling response of doubly curved shell panels on rectangular planform. These have been addressed in the present study. First, in this work general 9- and 16-noded isoparametric mixed interpolation of tensorial components (MITCs) degenerated shell elements are developed for the nonlinear analysis of composite shell panels. The structural model is based on a first-order shear deformation theory incorporating geometric nonlinearities. However, geometric imperfections are not considered in the analysis. Next, the nonlinear response of graphite/epoxy laminated doubly curved shell panels having rectangular planform subjected to thermomechanical loads are obtained considering temperature-dependent thermal and elastic properties of composite material. The first-ply failure of laminates is predicted with the Tsai–Wu failure criterion. In the end, numerical results are presented showing the effect of temperature degradation of mechanical properties on limit loads, failure loads, and snap-through response of shallow curved panels.

Finite Element Formulation

The global coordinates (${}^{t}x_i$, $i = 1, 3$) of a generic point at time t in the shell element (Fig. 1) undergoing very large displacements and rotations can be expressed as[17]

$$ {}^{t}x_i = \sum_{k=1}^{N} N_k\, {}^{t}x_i^k + \frac{t}{2}\sum_{k=1}^{N} h_k N_k\, {}^{t}\boldsymbol{V}_{ni}^k \tag{1} $$

where N_k are interpolation functions associated with node k; ${}^{t}x_i^k$ are global coordinates of node k at time t, $i = 1, 2, 3$; h_k is the shell thickness at node k; and ${}^{t}V_{ni}^k$ is normal to the shell midsurface at

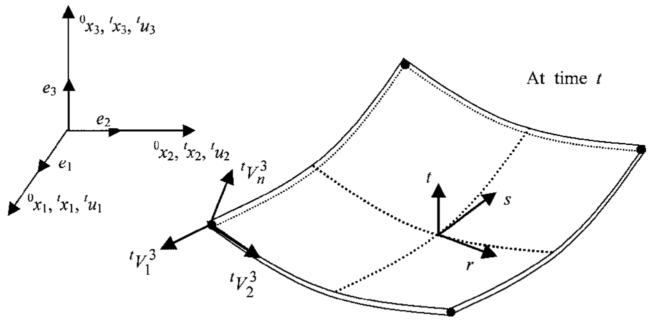

Fig. 1 Geometry of degenerated shell element with coordinate axes at time *t*.

node k of the N-noded ($N = 9, 16$) isoparametric finite element. The displacement components at time t (${}^{t}u_i$, $i = 1, 3$) and the increment in displacement components from time t to $t + \Delta t$ (u_i, $i = 1, 3$) are expressed as

$$ {}^{t}u_i = {}^{t}x_i - {}^{0}x_i = \sum_{k=1}^{N} N_k\, {}^{t}u_i^k + \frac{t}{2}\sum_{k=1}^{N} h_k N_k \left({}^{t}V_{ni}^k - {}^{0}V_{ni}^k\right) \tag{2} $$

$$ u_i = {}^{t+\Delta t}x_i - {}^{t}x_i = \sum_{k=1}^{N} N_k\, {}^{t}u_i^k + \frac{t}{2}\sum_{k=1}^{N} h_k N_k V_{ni}^k \tag{3} $$

where

$$ V_{ni}^k = {}^{t+\Delta t}V_{ni}^k - {}^{t}V_{ni}^k \tag{4} $$

Now the changes in direction cosines of the shell normal, given by V_{ni}^k may be expressed in terms of rotations (α_k and β_k) about two vectors ${}^{t}\boldsymbol{V}_1^k$ and ${}^{t}\boldsymbol{V}_2^k$ that are orthogonal to ${}^{t}V_{ni}^k$ at time t. In the updated Lagrangian formulation, the equation of equilibrium with incremental decomposition of stresses and strains is written as

$$ \int_{{}^{t}V} {}_{t}S_{ij}\,\delta_{t}\varepsilon_{ij}\,\mathrm{d}^{t}V + \int_{{}^{t}V} {}^{t}\tau_{ij}\,\delta_{t}\eta_{ij}\,\mathrm{d}^{t}V = {}^{t+\Delta t}\Re - \int_{{}^{t}V} {}^{t}\tau_{ij}\,\delta_{t}\varepsilon_{ij}\,\mathrm{d}^{t}V \tag{5} $$

where the stresses are ${}^{t+\Delta t}_{t}S_{ij} = {}^{t}\tau_{ij} + {}_{t}S_{ij}$ and ${}^{t}_{t}S_{ij} \cong {}^{t}\tau_{ij}$ and the strains are ${}^{t+\Delta t}_{t}\varepsilon_{ij} = {}_{t}\varepsilon_{ij}$ and ${}_{t}\varepsilon_{ij} = {}_{t}e_{ij} + {}_{t}\eta_{ij}$, ${}^{t+\Delta t}_{t}S^{ij}$ are the contravariant components of the second Piola–Kirchhoff stress tensor including the thermal stresses, and ${}^{t+\Delta t}\Re$ is the virtual work of the applied loads. Furthermore, ${}_{t}e_{ij}$ and ${}_{t}\eta_{ij}$ are the linear and nonlinear strains, respectively, and ${}^{t}\tau_{ij}$ are the Cauchy stress components. In the updated Lagrangian formulation the covariant components of the Green–Lagrange strain tensor ε_{ij}^{DI} may be written as

$$ {}^{t+\Delta t}_{t}\varepsilon_{ij}^{\mathrm{DI}} = \tfrac{1}{2}\left({}^{t+\Delta t}\boldsymbol{g}_i\, {}^{t+\Delta t}g_j - {}^{t}\boldsymbol{g}_i\, {}^{t}g_j\right) \tag{6} $$

where the superscript DI indicates that the strains are obtained by direct interpolation by using the finite element displacement assumptions and ${}^{t+\Delta t}\boldsymbol{g}_i$ and ${}^{t}\boldsymbol{g}_i$ are the covariant base vectors[17,18] associated with convected coordinates r_i at times t and $t + \Delta t$, respectively. This coordinate system is defined element-wise by the element isoparametric coordinates r, s, t ($r_1 = r$, $r_2 = s$, $r_3 = t$).

The linear and nonlinear parts of the strain ${}_{t}\varepsilon_{ij}^{\mathrm{DI}}$ may be written respectively as

$$ {}_{t}e_{ij} = \frac{1}{2}\left(\frac{\partial^{t}u}{\partial r_i}\cdot {}^{t}g_j + \frac{\partial^{t}u}{\partial r_j}\cdot {}^{t}g_i\right) \tag{7} $$

$$ {}_{t}\eta_{ij} = \frac{1}{2}\left(\frac{\partial^{t}u}{\partial r_i}\cdot\frac{\partial^{t}u}{\partial r_j}\right) \tag{8} $$

The mixed interpolated elements are constructed by using the assumed strain fields $\varepsilon_{ij}^{\mathrm{AS}}$ in place of $\varepsilon_{ij}^{\mathrm{DI}}$. Here the subscripts and superscripts relating to time (t to $t + \Delta t$) are omitted for clarity. The covariant strain components $\varepsilon_{ij}^{\mathrm{AS}}$ are defined as

$$\varepsilon_{ij}^{\mathrm{AS}}(r, s, t) = \sum_{k=1}^{n_{ij}} N_k^{ij}(r, s)\varepsilon_{ij}^{\mathrm{DI}}(r, s, t) \tag{9}$$

where $N_k^{ij}(r, s)$ are interpolation functions (polynomials in r and s) associated with the strain component ε_{ij} at tying point k and n_{ij} is the number of tying points described in Refs. 17 and 18. After simplification, the incremental linearized finite element equilibrium equation may be written as

$$\left[{}_n^nK_L\right]\{d\} + \left[{}_n^nK_{\mathrm{NL}}\right]\{d\} = \{\boldsymbol{F}\} - \left\{{}_n^n\boldsymbol{F}\right\} \tag{10}$$

where $[{}_n^nK_L]$ is the linear strain incremental stiffness matrix, $[{}_n^nK_{\mathrm{NL}}]$ is the nonlinear strain (geometric or initial stress) incremental stiffness matrix, $\{\boldsymbol{F}\}$ is the load vector, and $\{{}_n^n\boldsymbol{F}\}$ is the vector of nodal point forces equivalent to element stresses at the nth equilibrium state. The stiffness matrices are evaluated with full numerical integration; that is, 3×3 Gauss integration in the r–s plane is used for the 9-noded shell element and 4×4 Gauss integration for the 16-noded element.

The nonlinear governing equilibrium equation (10) is solved with the central displacement (w_{central}) as an independent variable.[19] In this paper, the average displacement (w_{av}) is also computed together with nondimensional central displacement w_c ($=w_{\mathrm{central}}/h$) and presented with nondimensional load parameter P for uniformly distributed lateral pressure and Q for a central concentrated load. The average displacement w_{av} and the load parameter are defined as follows:

$$w_{\mathrm{av}} = \frac{1}{ab}\int_0^a \int_0^b \frac{w}{h}\,\mathrm{d}x\,\mathrm{d}y \tag{11}$$

$$P = \frac{q_0 R_x^2}{E_2 h^2} \tag{12}$$

$$Q = \frac{P_c R_x^2}{abE_2 h^2} \tag{13}$$

where q_0 is the intensity of the uniformly distributed lateral pressure and P_c is the central point load. The results of the next section are obtained by considering immovable hinged boundary conditions along the supports, that is, $u = v = w = 0$.

Results and Discussion

In this section, the computer code developed for the nonlinear response analyses of shells is verified against available results in the literature. The displacement-control method[19] was used to solve the nonlinear finite element equilibrium equations. After validating the present formulation, new results are presented for 8-layered cross-ply [0/90 deg]$_{2s}$ graphite/epoxy laminates. In all of these figures, the response of shell panels subjected to mechanical loads, thermal loads, and thermomechanical loads are presented. At the end, the lamina failure is predicted with the Tsai–Wu failure criterion. The load vs average displacement (w_{av}) paths are plotted by solid lines and the load vs central displacement (w_c) paths are plotted by dotted lines. The mechanical and elastic properties used in the analyses are given in Tables 1 and 2 (Ref. 20). The results were obtained by discretizing one quarter of the shell panel with a 2×2 mesh, using a 16-noded MITC element.

Validation

The nondimensional central deflection w_c of a simply supported four-layered [0/90/90/0 deg] laminated composite spherical shell panel under uniformly distributed load q_0 are compared with those of Reddy[21] (Table 3). The material properties are also given in Table 3. The maximum difference of 4% in nondimensional central displacement is observed in the case of a deep ($R/a = 2$) thick shell. The nondimensional central deflections w_c of this composite shell panel are obtained using the present 9-node shell element with a 3×3 mesh size and 16-node shell element with a 2×2 mesh size for one quarter of the shell panel. Both 9-node and 16-node elements perform very well in the case of shallow thin as well as shallow thick spherical shell panels as observed from Table 3.

The numerical results of nonlinear analysis of an isotropic hinged spherical cap under uniformly distributed load are compared with those of Leicester[22] in Fig. 2 for two different values of c/h (where c represents the maximum rise of the spherical cap and h is the thickness of the spherical cap). The present result is obtained using a 16-node shell element with a 2×2 mesh size for one quarter of the shell panel. It is observed from visual inspection that results compare well.

Table 1 Temperature-dependent mechanical properties of graphite/epoxy composites ($G_{13} = G_{23} = G_{12}$)[20]

Temperature, °C	20	200	260	600
E_1, GPa	141	141	141	141
E_2, GPa	13.1	10.3	0.138	0.0069
G_{12}, GPa	9.31	7.45	0.069	0.0034
ν_{12}	0.28	0.28	0.28	0.28
α_1, 10^{-6}/°C	0.018	0.054	0.054	0.054
α_2, 10^{-6}/°C	21.6	37.8	37.8	37.8

Table 2 Temperature-dependent strengths of graphite/epoxy composites ($X_c = X_t$, $R = S = T$)[20]

Temperature, °C	X_t, MPa	Y_t, MPa	Y_c, MPa	S, MPa
20	1650	58.9	236	106
200	1650	46.5	186	84
260	↓	0.0	0.0	0.0
740	330	0.0	0.0	0.0

Table 3 Nondimensional center deflection $\bar{w}_c$ vs radius-to-span ratio (R/a) of a four-layered [0/90/90/0 deg] spherical shell under uniformly distributed load for two different thicknesses ($E_1 = 25E_2$, $G_{23} = 0.2E_2$, $G_{13} = G_{12} = 0.5E_2$, $\nu_{12} = 0.25$)

	$a/h = 100.0$			$a/h = 10.0$		
	Present study			Present study		
R/a	9-Node element (3×3)	16-Node element (2×2)	Ref. 21	9-Node element (3×3)	16-Node element (2×2)	Ref. 21
2	0.2822	0.2825	0.2844	7.6448	7.6489	8.0517
3	0.6211	0.6216	0.6246	8.9215	8.9713	9.1463
4	1.0516	1.0522	1.0559	9.4409	9.4497	9.5999
5	1.5313	1.5318	1.5358	9.7553	9.7787	9.8249
10	3.7170	3.7174	3.7208	10.1516	10.1609	10.1410
10^{30}	6.8376	6.8360	6.8331	10.3748	10.3837	10.2510

$\bar{w}_c = wh^3E_2/q_0a^4 \times 10^3$, $q_0 =$ uniformly distributed load, h is the thickness of the shell.

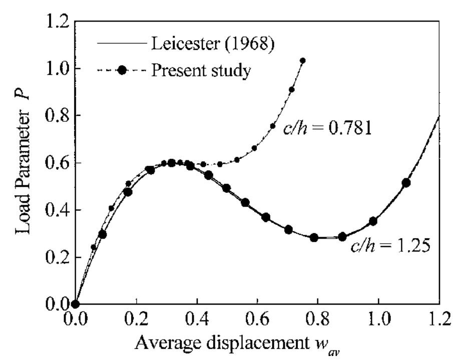

Fig. 2 Deformation w_{aw} of an isotropic hinged spherical shell with different c/h ratio.

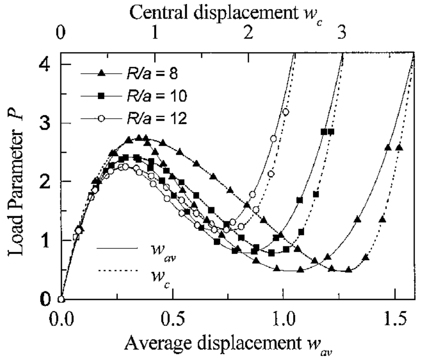

Fig. 3 Effect of radius-to-span ratio on the nonlinear behavior of graphite/epoxy composite spherical shell panels under uniformly distributed load ($R_x = R_y$, $a = b$, $a/h = 100.0$).

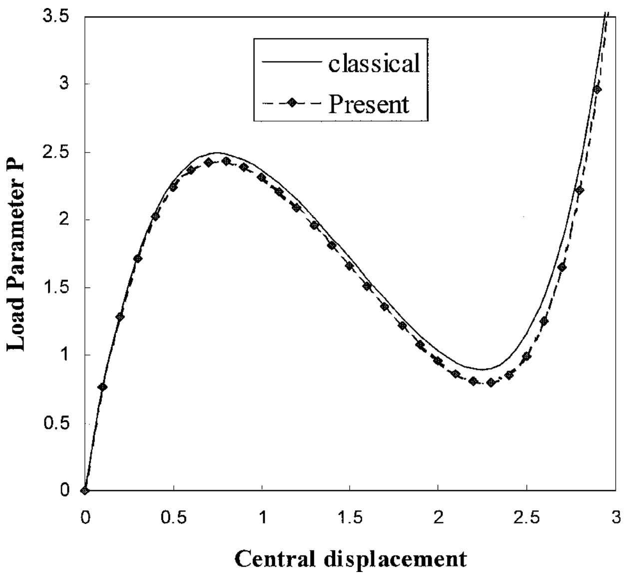

Fig. 4 Effect of shear deformation on the nonlinear behavior of an eight-layered [0/90 deg]$_{2s}$ graphite/epoxy doubly curved panel under uniformly distributed load ($R_x = R_y$, $= 1000h$, $a = b = 100h$).

Response of Doubly Curved Shell Panels Subjected to Only Mechanical Loads

Nonlinear equilibrium paths of thin ($a/h = 100.0$) eight-layered [0/90 deg]$_{2s}$ graphite/epoxy hinged ($u = v = w = 0$ along the edges) spherical shell panels under uniformly distributed lateral pressure q_0 are presented in Fig. 3 for three different values of radius-of-curvature-to-span ratio ($R/a = 8, 10, 12$). From Fig. 3, it is observed that initially the shell displacement increases with the increase of load and reaches the limit point for all the cases considered here. Afterward, it shows a typical snap-through behavior for all R/a ratios considered here. It is also observed that the deep shell panels with a lower R/a ratio have higher limit load and shallow shell panels with higher R/a ratio have comparatively lower limit load. However, after the limit point the displacement increases significantly for the deep shell panels ($R/a = 8$) compared to shallow ones ($R/a = 12$). It is observed from Fig. 3 that both the load vs average displacement and the load vs central displacement curves follow the same trend. However, it may be observed that for the same load parameters, central deflection is almost 1.8–2.0 times the average displacement, indicating that the central portion deflects much more than the remaining portion of the shell. The effect of shear deformation on the nonlinear response of eight-layered [0/90 deg]$_{2s}$ graphite/epoxy doubly curved shell panel ($a = b = 100h$, $R_x = R_y = 100h$) subjected to mechanical load is shown in Fig. 4. It may be observed from the figure that the transverse shear deformation reduces the limit load marginally for the shell panel considered here.

Figure 5 shows the nonlinear behavior of thin ($a/h = 100.0$), shallow ($R_x/a = 10.0$), hinged composite cross-ply doubly curved elliptic paraboloid shell panels under uniformly distributed load q_0 for different values of curvature ratios (R_x/R_y). It may be observed from Fig. 5 that the panels having a lower value of radius of curvature R_y show comparatively higher limit load. However, after the limit point the displacements increase at a faster rate compared to other shell configurations. Moreover, the limit point occurs for all the cases at the same value of average and central displacement.

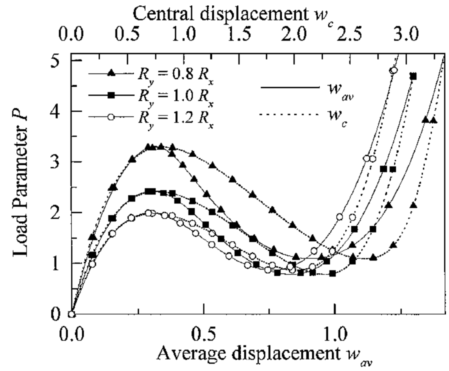

Fig. 5 Effect of curvature ratio on the nonlinear behavior of graphite/epoxy composite hinged elliptic paraboloid shell panels under uniformly distributed load ($a = b$, $a/h = 100.0$, $R_x/a = 10$).

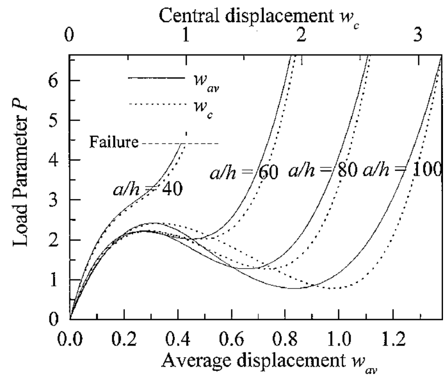

Fig. 6 Effect of thickness-to-span ratio on the nonlinear behavior of graphite/epoxy composite spherical shell panels under uniformly distributed load ($a = b$, $a/h = 100.0$, $R_x/a = 10$).

Nonlinear behavior of shallow ($R_x/a = 10.0$) composite cross-ply hinged spherical shell panels under uniformly distributed mechanical load q_0 are presented in Fig. 6 for different values of span-to-thickness (a/h) ratios. It is observed from Fig. 6 that the thin panels ($a/h = 60, 80, 100$) show a softening type (snap through) of behavior, whereas the thick panels ($a/h = 40$) show a stiffening type of behavior. However, in the case of shell panels with $a/h = 60.0$, the softening type of behavior is not pronounced. In the case of thick panels ($a/h = 40$) the laminate failure is observed to be due to excessive stress at the center. The failure occurs at a central displacement (w_c/h) of around 1.0 and is predicted by the Tsai–Wu failure criterion.

Response of Doubly Curved Shell Panels Subjected to Only Thermal Loads

Figure 7 shows the behavior of eight-layered [0/90 deg]$_{2s}$ shallow graphite/epoxy spherical shell panels subjected to uniform temperature rise for different cases of span-to-thickness (a/h) ratios. Temperature-dependent material properties are used in the analysis. The shell deformation is found to increase with the increase in temperature up to 200°C, after which the shell deformation decreases with the increase of temperature. After 200°C, the equivalent mechanical load reduces due to the degradation of material properties (Table 1). Here composite laminates are treated as purely elastic material; that is, the deflection decreases when the load is removed. Hence, due to reduction in thrust, the displacement reduces beyond 200°C. It is worth mentioning that the displacements due to the temperature rise are always upward.

Response of Doubly Curved Shell Panels Subjected to Thermomechanical Loads

The nonlinear equilibrium paths of graphite/epoxy doubly curved shell panels under combined thermal and mechanical loads are presented in Fig. 8. Four carefully selected test problems with different geometrical parameters are considered, as shown in Table 4.

Temperature-dependent material properties are used in the analysis. Four different temperature loadings are considered in addition to the uniformly distributed mechanical load: 0, 30, 50, and 70°C. In all four cases considered here, higher thermal load gives higher limit point load. The first case (Fig. 8a) shows softening behavior whereas the last two cases (Figs. 8c and 8d) show a hardening type of response. Moreover, in the second case without thermal load (Fig. 8b), no snap-through buckling is observed. As the thermal load is increased, the shell shows a softening type of behavior. It is observed from the preceding figures that, by suitably adjusting geometric properties, one can avoid snap-through buckling altogether. Moreover, in the last two cases the lamina failure is observed. The failure is initiated at the center of the panel due to excessive stress. This failure is predicted by the Tsai–Wu failure criterion.

Next an attempt has been made to understand the effect of degradation of mechanical properties due to temperature rise on the limit load and response of composite shells in general. The nonlinear equilibrium paths of graphite/epoxy doubly curved shell panel ($a = b = 80h$, $R_x = R_y = 800h$) under combined thermal and mechanical loads are traced for both temperature-dependent and temperature-independent material properties in Fig. 9. Two different

Table 4 Selected test problems

Configuration	a	b	R_x	R_y
a	$80h$	$80h$	$800h$	$800h$
b	$60h$	$60h$	$600h$	$800h$
c	$40h$	$60h$	$400h$	$800h$
d	$40h$	$40h$	$400h$	$400h$

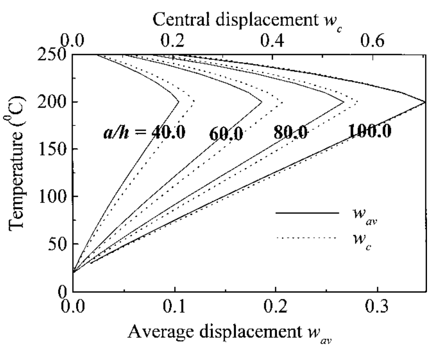

Fig. 7 Nonlinear behavior of graphite/epoxy shallow spherical shell under uniform temperature rise ($R_x/a = 10$, $R_x = R_y$, $a = b$, $a/h = 100.0$).

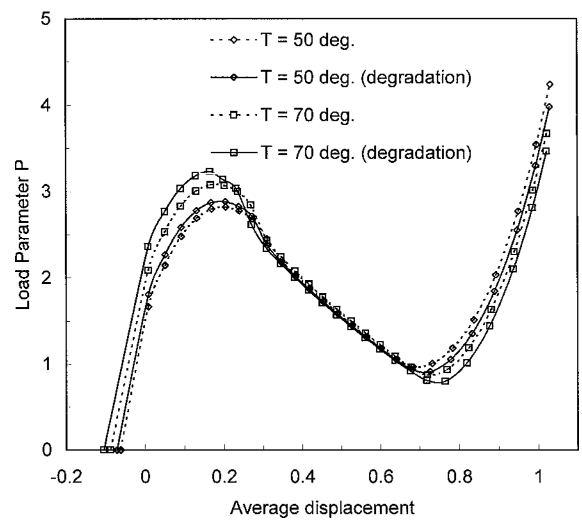

Fig. 9 Nonlinear equilibrium path of an eight-layered [0/90 deg]$_{2s}$ doubly curved shell panel ($a = b = 80h$, $R_x = R_y = 800h$) under uniformly distributed load.

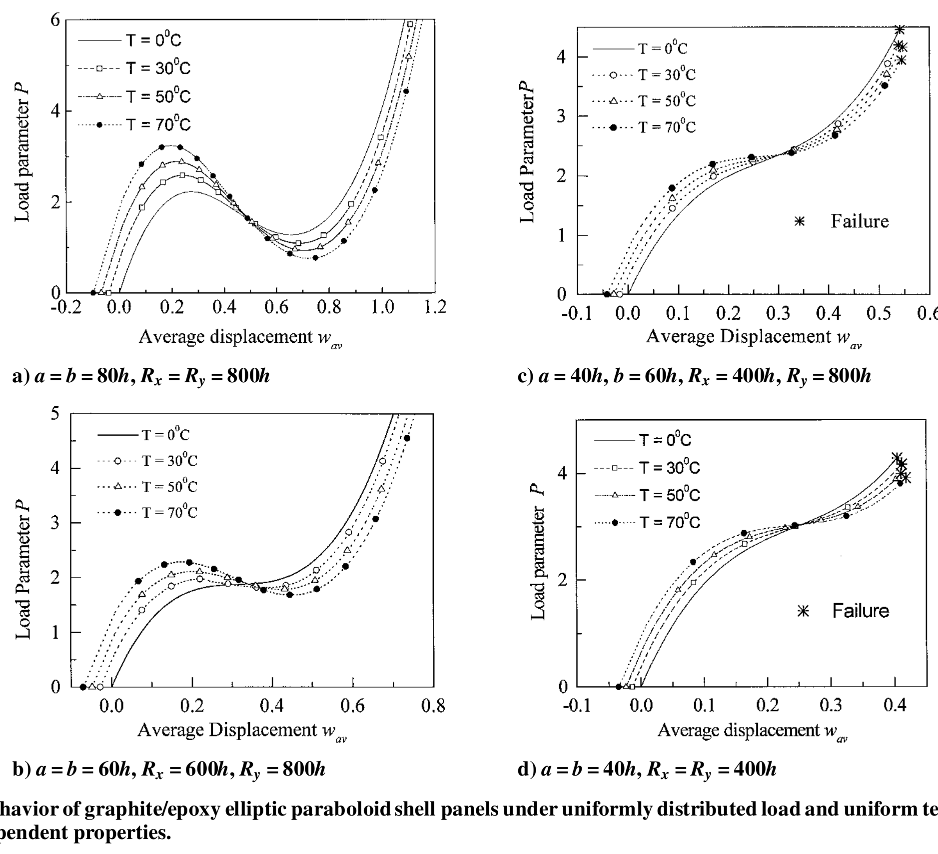

Fig. 8 Nonlinear behavior of graphite/epoxy elliptic paraboloid shell panels under uniformly distributed load and uniform temperature distribution with temperature-dependent properties.

temperature loadings are considered: 50 and 70°C. From the results, it is clear that the temperature-dependent material properties increase the limit load.

Conclusions

The higher order (9- and 16-noded) MITC shell element, initially developed by Bucalem and Bathe[18] for the nonlinear analysis of isotropic shell panels under mechanical loads has been extended for the case of laminated composite shell panels under combined thermal and mechanical loads. Temperature-dependent and -independent material and thermal properties are used in the analysis. The nonlinear behavior of composite shell panels subjected to uniformly distributed lateral pressure, uniform temperature rise, or both mechanical and thermal loads are studied.

The thin panels show a softening behavior (snap-through phenomenon), whereas the thick panels show a stiffening behavior under mechanical load alone for the case of doubly curved panels. The variations of central displacement and average displacement with load are similar in nature. For the cases of shell panels under thermal load only, no instability is observed over the temperature range considered.

In the case of shell panels subjected to both temperature and mechanical loads, the increase in temperature increases the load-carrying capacity up to a limit point. However, after snap-through buckling this trend is reversed. In the presence of thermal loads along with the mechanical loads, the shell shows a softening type of behavior even in cases where snap-through buckling is not observed due to mechanical loads alone. It is observed from the present work that by suitably adjusting geometric properties one can avoid snap-through buckling altogether. The transverse shear deformation reduces the limit load marginally for the present case. Also, it is observed from the cases considered in this Paper that the temperature-dependent material properties increase the limit load. In the case of thick panels, the laminate failure is observed due to excessive stress at the center.

Acknowledgments

The authors sincerely thank the reviewers for their comments, which helped in improving the manuscript.

References

[1]Thangaratnam, K. R., Palaninathan, R., and Ramachandran, J., "Thermal Buckling of Laminated Composite Shells," *AIAA Journal*, Vol. 28, 1990, pp. 859–860.

[2]Eslami, M. R., Ziaii, A. R., and Ghorbanpour, A., "Thermoelastic Buckling of Thin Clindrical Shells Based on Improved Stability Equations," *Journal of Thermal Stresses*, Vol. 19, 1996, pp. 299–315.

[3]Eslami, M. R., and Javaheri, R., "Buckling of Composite Cylindrical Shells Under Mechanical and Thermal Loads," *Journal of Thermal Stresses*, Vol. 22, 1999, pp. 527–545.

[4]Krizhevsky, G., and Stavsky, Y., "Refined Theory for Non-Linear Buckling of Heated Composite Shallow Spherical Shells," *Computers and Structures*, Vol. 55, 1995, pp. 1007–1014.

[5]Huang, N. N., and Tauchert, T. R., "Large Deflections of Laminated Cylindrical and Doubly Curved Panels Under Thermal Loading," *Computers and Structures*, Vol. 41, No. 2, 1991, pp. 303–312.

[6]Huang, N. N., and Tauchert, T. R., "Thermal Stresses in Doubly-Curved Cross-Ply Laminates," *International Journal of Solids and Structures*, Vol. 29, 1992, pp. 991–1000.

[7]Birman, V., and Bert, C. W., "Buckling and Post-Buckling of Composite Plates and Shells Subjected to Elevated Temperature," *Journal of Applied Mechanics*, Vol. 60, 1993, pp. 514–519.

[8]Librescu, L., and Souza, M. A., "Post-Buckling of Geometrically Imperfect Shear-Deformable Flat Panels Under Combined Thermal and Compressive Edge Loadings," *Journal of Applied Mechanics*, Vol. 60, 1993, pp. 526–533.

[9]Librescu, L., Lin, W., Nemeth, M. P., and Starnes, J. H., "Thermomechanical Postbuckling of Geometrically Imperfect Flat and Curved Panels Taking into Account Tangential Edge Constraints," *Journal of Thermal Stresses*, Vol. 18, 1995, pp. 465–482.

[10]Shen, H., "Thermo Mechanical Postbuckling of Stiffened Cylindrical Shell," *Journal of Engineering Mechanics*, Vol. 123, 1997, pp. 433–443.

[11]Noor, A. K., and Peters, J. M., "Analysis of Composite Panels Subjected to Thermo-Mechanical Loads," *Journal of Aerospace Engineering*, Vol. 12, 1999, pp. 1–7.

[12]Hause, T., Johnson, T. F., and Librescu, L., "Effect of Face Sheet Anisotropy on Buckling and Postbuckling of Sandwich Plates," *Journal of Spacecraft and Rockets*, Vol. 37, 2000, pp. 331–341.

[13]Librescu, L., Nemeth, M. P., Starnes, J. H., and Lin, W., "Nonlinear Response of Flat and Curved Panels Subjected to Thermo-Mechanical Loads," *Journal of Thermal Stresses*, Vol. 23, 2000, pp. 549–582.

[14]Noor, A. K., and Burton, W. S., "Computational Models for High-Temperature Multilayered Composite Plates and Shells," *Applied Mechanics Reviews*, Vol. 45, 1992, pp. 419–445.

[15]Argyris, J., and Tenek, L., "Recent Advances in Computational Thermostructural Analysis of Composite Plates and Shells with Strong Nonlinearities," *Journal of Applied Mechanics*, Vol. 50, 1997, pp. 285–306.

[16]Thornton, E. A., "Thermal Buckling of Plates and Shells," *Applied Mechanics Reviews*, Vol. 46, 1993, pp. 485–506.

[17]Bathe, K. J., *Finite Element Procedures*, Prentice–Hall, Englewood Cliffs, NJ, 1996.

[18]Bucalem, M. L., and Bathe, K. J., "Higher-Order MITC General Shell Elements," *International Journal for Numerical Methods in Engineering*, Vol. 36, 1993, pp. 3729–3754.

[19]Batoz, J. L., and Dhatt, G., "Incremental Displacement Algorithm for Non-Linear Problems," *International Journal for Numerical Methods in Engineering*, Vol. 14, 1979, pp. 1262–1267.

[20]Chen, J. K., Sun, C. T., and Chang, C. I., "Failure Analysis of a Graphite/Epoxy Laminate Subjected to Combined Thermal and Mechanical Loading," *Journal of Composite Materials*, Vol. 19, 1985, pp. 408–423.

[21]Reddy, J. N., "Solutions of Moderately Thick Laminated Shells," *Journal of Engineering Mechanics*, Vol. 110, 1984, pp. 794–809.

[22]Leicester, R. H., "Finite Deformations of Shallow Shells," *Journal of Engineering Mechanics*, Vol. 94, 1968, pp. 1409–1423.

K. N. Shivakumar
Associate Editor